HHS Public Access

Author manuscript

Nat Chem. Author manuscript; available in PMC 2015 November 01.

Published in final edited form as:

Nat Chem. 2015 May ; 7(5): 438–446. doi:10.1038/nchem.2236.

Functionalization of Cobalt Porphyrin-Phospholipid Bilayers with His-tagged Ligands and Antigens

Shuai Shao[1,2], **Jumin Geng**[1], **Hyun Ah Yi**[3], **Shobhit Gogia**[2], **Sriram Neelamegham**[2], **Amy Jacobs**[3], and **Jonathan F. Lovell**[1,2,*]

[1]Department of Biomedical Engineering, University at Buffalo, State University of New York, Buffalo, New York 14260, USA

[2]Department of Chemical and Biological Engineering, University at Buffalo, State University of New York, Buffalo, New York 14260, USA

[3]Department of Microbiology and Immunology, University at Buffalo, State University of New York, Buffalo, New York 14260, USA

Abstract

Methods to attach polypeptides to lipid bilayers are often indirect, ineffective and can represent a substantial bottleneck in the formation of functionalized lipid-based materials. Although the polyhistidine tag (his-tag) has been transformative in its simplicity and efficacy in binding to immobilized metals, the successful application of this approach has been challenging in physiological settings. Here we show that lipid bilayers containing porphyin-phospholipid that is chelated with cobalt, but not other metals, can effectively capture his-tagged proteins and peptides. The binding follows a Co(II) to Co(III) transition and occurs within the sheltered hydrophobic bilayer, resulting in essentially irreversible attachment in serum or in million-fold excess of competing imidazole. Using this approach we anchored homing peptides into the bilayer of preformed and cargo-loaded liposomes to enable tumour-targeting without disrupting the bilayer integrity. As a further demonstration, a synthetic HIV-derived protein fragment was bound to immunogenic liposomes for potent antibody generation for an otherwise non-antigenic peptide.

Introduction

The development of targeted nanoparticles that nimbly guide payloads to diseased tissues[1], and the rational design of peptide antigens that induce the immune system to combat diseases[2] have been the focus of considerable research efforts. One bottleneck in advancing these techniques stems from difficulties in easily and reliably attaching peptides and proteins to larger scaffolds; targeted nanoparticles require effective ligands and unconjugated

*jflovell@buffalo.edu.

Author contributions

S.G. and S.N. designed and produced the his-tagged fluorescence protein reporter. S.S. performed synthesis, chemical characterization, binding, targeting and immunization experiments. J.G. led animal experiments. A.J. and H.A.Y. carried out HIV entry inhibition experiments. S.S. and J.F.L. conceived the project, interpreted the data and wrote the manuscript.

peptides themselves are weakly immunogenic. Bioconjugate chemistry has provided a range of strategies[3], but most nanoparticulate conjugations suffer from limitations relating to one or more of the following: 1) low conjugation yields and necessitated purification steps; 2) incompatibility with biological buffers, making labeling of intact nanoparticles impossible; 3) variable labeling sites and conjugated polypeptide conformations, creating an inhomogeneous particle population with varying degrees of function; 4) necessity for complex and exogenous chemical approaches.[4]

Standard approaches for ligand attachment to aqueous nanoparticles make use of maleimides, succinimidyl esters and carboiimide-activated carboxylic acids.[5] These can covalently react with amine and thiol groups of polypeptides. The use of maleimide-lipids has been explored extensively for antibody-conjugated immunoliposomes.[6] Conjugation yields may reach as high as 90% from an overnight reaction, but subsequent quenching of free maleimide groups and additional purification is required.[7] Proteins may require a preparative step of thiolation and purification prior to conjugation.[8] Antibody orientation is a major factor influencing the conjugated antibody target binding efficacy, but these approaches result in numerous antibody labeling sites and indiscriminate orientations.[9] Biorthogonal synthetic strategies such as the click reaction have recently been applied to preformed liposomes, however these require the use exogenous catalysts and unconventional amino acids.[10]

Another approach that is suitable for smaller peptides which are less prone to permanent denaturation in organic solvents is to conjugate the peptides to a lipid anchor. The resulting lipopeptides can then be incorporated along with the other lipids during the liposome formation process. This approach has been used to generate synthetic vaccines that induce antibody production against otherwise non-immunogenic peptides.[11] However, due to their amphipathic character, in that case the lipopeptides proved difficult to purify. It has also been shown that lipopeptides do not fully incorporate into liposomes during the formation process, resulting in aggregation.[12] These problems have necessitated evolving strategies for working with liposomal lipopeptides such as adding multiple lipidation sites.[13]

One alternate strategy of interest that could avoid these limitations would be to adopt the non-covalent paradigm used in immobilized metal ion affinity chromatography (IMAC).[14] Polypeptides containing a polyhistidine-tag (his-tag) comprising a stretch of approximately 6–10 consecutive histidine residues can be purified from a crude lysate using immobilized microparticles decorated with Ni, Zn or Co chelators such as nitrilotriacetic acid (NTA). This approach has changed the face of biotechnology and is common practice for the purification of recombinant proteins.[15,16] Ni-NTA conjugated phospholipids, which were described over 20 years ago and are commercially available, have also been used to bind his-tagged proteins, but largely in the context of structural biology studies.[17–19] Unfortunately, the chelation of his-tagged proteins with various Ni-NTA lipids in nanoparticulate form is not stable in biological media such as serum.[20,21] Based on the suitability of lipids for use *in vivo* in the form of liposomes or as coatings for other nanoparticles[22], stable lipid-based polyhistidine-binding would be enabling for applications in biological settings.

Porphyrin-phospholipid (PoP) conjugates have recently been developed that can self-assemble into biodegradable nanovesicles for multimodal imaging and phototherapy.[23–26] With its 4 cyclic nitrogen atoms, PoP also represents a potent chelator for the exact same transition metals that are frequently used in IMAC. In this work, we demonstrate that a metallo-PoP bilayer specifically formed from cobalt porphyrin-phospholipid (Co-PoP) can stably bind his-tagged polypeptides with simple aqueous incubation (Fig. 1a). This represents a new binding paradigm, with the polyhistidine buried in the membrane phase, as the porphyrins themselves form the hydrophobic portion of the bilayer and are not accessible to the external aqueous environment (Fig. 1b). This leads to more stable binding, allows for significantly simpler non-covalent post-labeling paradigms following nanoparticle formation, and eliminates ambiguity regarding ligand orientation.

Results and Discussion

His-tagged protein binding to Co-PoP liposomes

A series of sn-1-palmitoyl sn-2-pyropheophorbide phosphtatidylcholine chelates was generated with the transition metals Co, Cu, Zn, Ni and Mn (Fig. 1c). PoP bilayers were then formed with 10 molar % metallo-PoP along with 85 molar % dioleoylphosphocholine (DOPC) and 5 molar % polyethylene glycol-conjugated distearoylphosphoethanolamine (PEG-lipid) via extrusion into 100 nm liposomes. His-tagged protein binding to PoP bilayers was assessed with a fluorescent protein reporter. As shown in Fig. 2a, the system comprised a fusion protein made up of two linked fluorescent proteins; Cerulean (blue emission) and Venus (green emission). Due to their linked proximity and spectral overlap, Cerulean serves as a Förster resonance energy transfer (FRET) donor for Venus, so that Cerulean excitation results in FRET emission from Venus. Cerulean was tagged at its C-terminus with a heptahistidine tag. However, if bound to a PoP bilayer, energy transfer from Cerulean is diverted to the bilayer itself, which is absorbing in the Cerulean emission range and thus competes with FRET to Venus. On the other hand, because Venus is not directly attached to the photonic bilayer, it is not completely quenched upon direct excitation, which enables tracking of the bound fusion protein.

A 3-color electrophoretic mobility shift assay (EMSA) was developed to assess reporter fusion protein binding to various PoP liposomes. 2.5 μg protein was incubated with the 50 μg of various PoP liposomes for 24 hours and then subjected to agarose gel electrophoresis. As shown in the top image in Fig. 2b, when the PoP-liposomes were imaged only the free base (2H) liposomes were readily visualized, along with the Zn-PoP liposomes to a lesser degree. This demonstrates that the metals have a quenching effect on the PoP and confirms they were stably chelated in the bilayer. As expected, the liposomes exhibited minimal electrophoretic mobility due to their relatively large size. Next, the same gel was imaged using Cerulean excitation and Venus emission to probe for inhibition of FRET, which would be indicative of the fusion protein binding to PoP liposomes. All the samples exhibited the same amount of FRET and migrated the same distance as the free protein with the exception of the protein incubated with Co-PoP liposomes, in which case FRET disappeared completely (middle image). To verify the presence of the protein, Venus was directly excited and imaged. Only with the Co-PoP liposomes was the reported protein co-localized

with the liposomes. Together, these images demonstrate that the protein bound quantitatively to Co-PoP liposomes. Solution-based studies confirmed this finding (Fig. 2c). Of all the types of PoP liposomes examined, only the Co-PoP ones induced a dramatic decrease in the FRET efficiency between Cerulean and Venus, due to liposomal binding. The binding required approximately a day to fully complete, although the time to achieve 50% binding (the $t_{1/2}$) was just 3 hours. It was previously shown by molecular dynamics simulations of a 2H-PoP bilayer that the center of the porphyrins (where metal chelation would occur) are inaccessible to the aqueous phase surrounding the bilayer.[25] Thus, this slow binding can be attributed to a his-tag that is partially obscured by the rest of the protein and has to make its way into the sheltered hydrophobic bilayer.

Polyhistidine Coordination with Co-PoP

The mechanism underlying his-tag binding to immobilized metals involves metal coordination with the nitrogenous imidazole groups of histidine residues. The absence of his-tag binding to liposomes formed with Ni(II), Cu(II), Zn(II) and Mn(II) PoP likely relates to axial ligand binding affinity or the coordination number within the porphyrin. For instance, it has been proposed that Ni(II) and Cu(II) porphyrin chelates can coordinate completely with the 4 surrounding macrocyclic nitrogens atoms without axial ligands.[27] For the Zn (II) and Mn (III) porphyrins, the ligand binding strength is likely insufficient to confer stable polyhistidine binding. Inorganic study of cobalt coordination was first pioneered by Alfred Werner over 100 years ago.[28] Co(III) complexes are of interest since they are often kinetically inert to ligand release and Co (III)-NTA has recently attracted interest for binding his-tag proteins with excellent stability.[29] Co(II) porphyrins, such as the originally synthesized Co-PoP, readily oxidize to Co(III) in aqueous solutions.[30] Confining Co (III)-mediated his-tag binding within a sheltered bilayer would be expected to further enhance binding stability in biological environments.

To determine the electronic state of the Co-PoP, paramagnetism was assessed. Because Co(II) is paramagnetic, but Co (III) porphyrins are low-spin and diamagnetic,[30] NMR was used to probe for peak broadening induced by paramagnetic species. As shown in Fig. 2d, based on the hydrogens of each carbon of the vinyl group within the PoP, wide peak broadening was observed only for the Co-PoP, and only in organic solvent. When Co-PoP was formed into aqueous liposomes, the peaks narrowed, indicative of oxidation to diamagnetic Co (III) within the bilayer. To further verify this mechanism, the reducing agent sodium sulfite was added to Co-PoP liposomes after they quantitatively bound a fluorescently-labeled his-tagged peptide. As shown in Fig. 2e, 2 M sulfite induced peptide release from Co-PoP liposomes. Liposomes were also formed with commercially available Ni-NTA lipid. The his-tagged peptide did not bind as avidly to the Ni-NTA liposomes. Upon addition of sulfite to the system, no release of the peptide was observed, as would be expected with Ni (II) which cannot readily be reduced. Together, these data suggest that Co-PoP transitions from Co (II) to Co (III) upon forming Co-PoP liposomes and the polyhistidine imidazole groups coordinate in the bilayer with chelated Co (III) in the PoP.

Stable his-tag binding to Co-PoP lipsoomes

The fluorescence reporter protein was then used to compare the binding of his-tagged proteins to liposomes incorporating either Co-PoP or Ni-NTA-lipid (Fig. 3a). Ni-NTA liposomes included 10 molar % 2H-PoP to enable protein binding determination based on FRET. By EMSA, the protein migrated unimpeded when incubated without liposomes or when incubated with 2H-PoP liposomes in both the FRET channel and protein channel. When incubated with Ni-NTA liposomes, migration of the protein was only slightly inhibited, indicating that the protein binding did not withstand the conditions of electrophoresis. The FRET channel was unquenched, confirming a lack of binding to the Ni-NTA liposomes. In contrast, when incubated with the Co-PoP liposomes, the protein stably bound with a complete disappearance of the FRET channel and decreased electrophoretic mobility that was consistent with the protein remaining bound to liposomes.

For biomedical applications, an intractable obstacle of using Ni-NTA-lipid is that it does not maintain stable his-tag binding in biological media such as serum.[20,21] To examine whether liposomes could maintain binding in the presence of serum, fetal bovine serum was added at a 1:1 volume ratio to a solution of liposomes that had bound the his-tagged protein. As shown in Fig. 3b, Ni-NTA liposomes did not fully sequester all the protein, which is consistent with the weak binding exhibited in the EMSA result. Following serum addition, all binding was abrogated over a 24 hour period. In the same conditions Co-PoP liposomes stably sequestered the his-tagged reporter protein without substantial protein release.

Since the histidine side chain comprises an imidazole group, an imidazole competition assay was used to compare the Ni-NTA and Co-PoP liposomes binding stability with his-tagged polypeptides. As shown in Fig. 3c, Co-PoP liposomes maintained over 75% binding to the reporter protein even at concentration approaching 1 M imidazole. This represents an approximate 10 million fold imidazole excess over the 100 nM protein concentration used in the binding study. In contrast, the Ni-NTA liposomes released over 90% the his-tag in the presence of just 30 mM imidazole. The drastically stronger binding of the Co-PoP liposome to the his-tag may be attributed to at least 2 factors; the superior stable chelation of Co(III) to imidazole groups and the protected hydrophobic environment of the Co-PoP bilayer which limits access to competing external molecules.

Liposomes formed with Ni-NTA-lipid, the cobalt-chelated Co-NTA-lipid, and Co-PoP could bind a fluorescent peptide in solution (Supplementary Fig. 1a). However, the binding of Co-NTA and Ni-NTA was not maintained during gel filtration chromatography (Supplementary Fig. 1b). Liposomes formed with Co-NTA and Ni-NTA, but not Co-PoP, released the peptide when incubated in serum (Supplementary Fig. 1c). This demonstrates the significance of bilayer-confined polyhistidine binding. We next examined whether or not Co-PoP was required for stable binding in serum, or whether a simple liposome-inserted cobalt porphyrin (Co-pyro) could be sufficient. After initial binding, incubation with serum caused the polypeptide to become displaced from the liposomes (Supplementary Fig. 2). This result is consistent with demonstrations that membrane-inserted porphyrins, but not PoP, rapidly exchange with serum components and exit the liposome.[25] Together these results point to the essential role of Co-PoP in order to stably bind his-tagged polypeptides.

Peptide binding to Co-PoP liposomes

Peptide targeting has attracted interest for use as disease and tissue-specific "zip codes".[31] The short RGD tripeptide, which is found in fibronectin and vibronectin, is a promising targeting ligand for its effective binding to the integrin $\alpha_V\beta_3$ expressed on tumor endothelial cells.[32,33] Co-PoP liposomes were examined to verify whether they can be delivered to molecular receptors on target cells via a his-tagged ligand approach with the short linear amino acid sequence GRGDSPKGAGAKG-HHHHHHH. Carboxy fluorescein (FAM) was labeled on the N-terminus to enable detection of binding to PoP-liposome via FRET. It has been shown that linear RGD peptides can be labeled with fluorophores without disrupting integrin binding.[34] As shown in Fig. 4a, when this peptide was incubated with various metallo-PoP liposomes, only the Co-PoP ones bound the peptide. Compared to protein-binding, peptide-binding was about five times faster. Presumably, the smaller size, faster molecular motion and decreased steric hindrance of the peptide enabled more rapid interdigitation into the bilayer to interact with and irreversibly bind the Co-PoP. Based on previous estimates that each ~100 nm liposome contains approximately 80,000 lipids,[7] this equates to 8000 Co-PoPs and 750 peptides per liposome. Since each peptide contained 7 histidine residues, the ratio of Co-PoP to histidine in the bilayer was 1:0.66. This represents an excess of Co-PoP and for conventional his-tag binding to Ni-NTA, of all the residues in the his-tag, just the ith and i+2 or i+5 histidine residues are believed to be involved in coordinating with the metal.[14] However, the porphyrin and polyhistidine density within the Co-PoP bilayer is likely higher and therefore the coordination mechanism may be different. Further work is required to determine the geometry and stoichiometry of his-tag binding in the Co-PoP bilayer phase.

The effect of his-tag length on peptide binding to Co-PoP liposome was examined. A series of N-terminus FAM-labeled peptides was synthesized with varying lengths of his-tag attached to the C-terminus. As demonstrated in Fig. 4b, when the his-tag was omitted from the peptide, no peptide binding was observed. With 2 histidine residues, the binding was slow, with a binding $t_{1/2}$ of nearly 10 hours. As the his-tag length increased, binding speed rapidly increased. With 6 residues, corresponding to the common hexahistidine tag, binding $t_{1/2}$ was less than one hour. By increasing the his-tag length to 10 residues, binding $t_{1/2}$ decreased to 20 minutes.

Next, lipid composition was varied to determine the effect of membrane fluidity on his-tag binding. Liposomes were formed with 90 molar % of either distearoylphosphatidylcholine (DSPC), distearoylphosphatidylcholine (DMPC) or DOPC along 10 molar % Co-PoP, Alternatively, 50 molar % cholesterol was also incorporated in the bilayer with a corresponding reduction in the amount of standard lipid used. DSPC forms rigid, gel-phase bilayers at room temperature, whereas DMPC and DOPC have lower transition temperatures and are in the liquid crystal phase at room temperature. Cholesterol occupies space in the bilayer and can have a moderating effect on membrane fluidity. Interestingly, no major differences were observed in the peptide binding rate to membranes of different compositions, with or without cholesterol, with binding $t_{1/2}$ values of under one hour (Fig. 4c) and the times required for binding 90 % of the peptide being between 10 to 12 hours (Supplementary Fig. 3). The peptide binding process might occur in a multi-step process so

that once the peptide begins insertion into the bilayer, cooperative effects of the polyhistidine are not impacted by lipid highly composition and fluidity. In the presence of 5 mg/mL bovine serum albumin (BSA), dramatic differences between the membranes with and without cholesterol were observed (Fig. 4d). The slower binding in cholesterol-free liposomes was likely due to greater interaction of BSA with the membrane interfering with peptide binding. Binding half-times were not reached with BSA at 50 mg/mL and serum completely inhibited binding (Supplementary Fig. 4).

Biotargeting of cargo-loaded liposomes

Given the binding efficacy of his-tagged peptides to Co-PoP liposomes, bilayer integrity was assessed to determine whether peptide binding induces membrane destabilization. The aqueous core of liposomes was loaded with the fluorophore sulforhodamine B, a water soluble dye, at self-quenching concentrations to probe for membrane permeabilization. As shown in Fig. 5a, dye-loaded liposomes did not release a substantial amount of dye over the 8 hour period in which the peptide had fully bound to the liposomes. At 24 hours, the Co-PoP liposomes with the peptide bound released less than 10% of the dye. Thus, his-tag insertion and binding is sufficiently gentle and non-disruptive so that the bilayer integrity and entrapped cargo remains intact. The analogous palmitoylated lipopeptide resulted in permeabilization of cargo-loaded liposomes upon incubation (Supplementary Fig. 5), further demonstrating the robustness of the his-tag approach.

Next, the liposomes were assessed for whether they could bind to their molecular targets with the established cell-line pair of U87 glioblastoma cells (RGD-binding) and MCF7 breast cancer cells (RGD non-binding).[35,36] Following sulforhodamine B entrapment, liposomes were first incubated with the his-tagged RGD peptide and then with both cell lines. Approximately 550 peptides were attached to each liposome. Liposomal uptake was assessed by examining the fluorescence in the cells following washing and lysis (to remove any effects of cargo self-quenching). As shown in Fig. 5b, high liposome uptake was observed in U87 cells incubated with targeted Co-PoP liposomes, whereas negligible binding occurred with MCF7 cells. As expected, without the RGD targeting ligand, no uptake occurred in either cell line. Inclusion of PEG-lipid in the liposome formulation resulted in liposomes that did not target to either cell line. It is likely that the presence of the PEG had an effect of obstructing the peptide, which is directly tethered to the bilayer surface. Binding could be inhibited with the presence of excess free RGD peptide, confirming the targeting specificity of the approach. Confocal microscopy substantiated these binding results (Fig. 5c). Although the FAM-labeled peptide was quenched by the PoP liposomes, sufficient signal remained to verify the binding of both the targeting peptide and the liposomal cargo. Both cargo and the peptide were internalized and remained co-localized in U87 cells. When the Co-PoP liposomes and targeting peptide were ad-mixed immediately prior to incubation with U87 cells, the targeting peptide itself bound to U87 cells but did not have time to attach to the liposomes, which remained untargeted. The same result was observed for 2H-PoP liposomes which did not bind the peptide. Peptide binding was maintained when liposomes were formed with only 1 molar % Co-PoP (Supplementary Fig. 6a) and maintained selective binding to U87 cells (Supplementary Fig. 6b). Cargo-loaded liposomes incubated a his-tagged cRGD moiety were intravenously injected into nude mice

bearing U87 tumors. As shown in Fig 5d, 45 minutes after intravenous injection, the targeted liposomes accumulated in tumors with 2.5 fold avidity compared to the untargeted liposomes. These data show that Co-PoP liposomes can be loaded with cargo in the core of the liposome, be labeled with a his-tagged targeting peptide without inducing cargo leakage, and be directed to molecular receptors expressed on cells expressing specific surface proteins in vitro and in vivo.

Liposomes represent only a subset of all the types of nanomaterials used in biomedical applications.[37] Co-PoP was assessed as a generalized surface coating with selective adhesion for his-tags. Gold nanoparticles were used as a model nanoparticle since these have been used in numerous biological applications.[38] Using an established protocol to lipid-coat gold nanospheres[39], a citrate-stabilized 60 nm gold dispersion was used to hydrate a thin film of PoP-lipid. Upon repeated centrifugation and re-suspension, the citrate was displaced, causing the nanospheres to aggregate (Supplementary Fig. 7a). However, in the presence of PoP-lipid, the nanospheres became coated and remained dispersible. Compared to citrate-stabilized gold, PoP-coated nanospheres had a slightly larger hydrodynamic size, due to the bilayer coating on the gold (Supplementary Fig. 7b). The presence of the coating following his-tag binding did not influence the plasmonic peak of the gold at 540 nm, demonstrating the mild nature of the ligand binding (Supplementary Fig. 7c). As shown in Supplementary Fig. 7d, only RGD-His Co-PoP-coated gold nanoparticles targeted U87 cells and free RGD inhibited the binding as determined by backscatter microscopy. Co-PoP gold alone, as well as 2H-PoP-coated gold incubated with the RGD-His peptide were ineffective at targeting U87 cells.

Development of antigenic liposomes

Many of the monoclonal antibodies that broadly neutralize HIV viral entry, such as 2F5, Z13 and 4E10, target a conserved linear epitope in the membrane proximal external region (MPER) of the gp41 envelope protein, making the MPER a prime target for HIV peptide vaccines.[40,41] However, it is exposed only during viral entry and attempts to use MPER peptides to generate neutralizing antibodies have faced challenges.[42,43] This has given rise to the paradigm that vaccination strategies should consider antibody interaction with the lipid bilayer in which the MPER is presented.[44] Recent efforts have made use of liposomes containing the Toll-like receptor 4 (TLR-4) agonist monophosphoryl lipid A (MPL) combined with liposome-bound MPER peptide sequences.[11,45,46] However, the use of a simple anchoring techniques based on binding of MPER his-tagged polypeptides to Ni-NTA liposomes generated low antibody titers.[47] We set out to examine if the same approach could be enhanced with Co-PoP liposomes.

A liposomal-peptide vaccination system was used with the MPER-His sequence NEQELLELDKWASLWNGGKGG-HHHHHHH. The MPER-His peptide was bound to Co-PoP liposomes containing MPL. A single injection containing 25 μg MPER-His and 25 μg of MPL was administered to BALB/c mice and to athymic nude mice. This elicited a titer on the order of 10^4 in both BALB/c mice and nude mice, demonstrating a strong humoral immune response (Fig. 6a). This may be significant since HIV infects helper T cell populations, making B cell mediated responses important. Following a booster injection, the

anti-MPER titer in athymic nude mice was unaffected, but in healthy mice there was a titer increase by an order of magnitude, demonstrating a T cell-mediated memory effect. Thus, the vaccination protocol resulted in both B cell and T cell-mediated immunity. Interestingly, a recent vaccination study using MPL liposomes and a lipid-anchored Alzheimer's-related peptide demonstrated a T cell-independent response, without any boosting phenomenon.[13] That study used subcutaneous injections and lower MPL doses (12 vs 25 μg) which may account for the different immune responses.

Next, various liposome and adjuvant components were examined to better determine the specificity of the immune response (Fig. 6b). The MPER-His peptide did not elicit any antibodies when injected on its own, in Freund's complete adjuvant or along with 2H-PoP liposomes containing MPL. When the peptide was administered with Co-PoP liposomes lacking MPL, no antibodies were generated whatsoever. Another lipid adjuvant, trehalose dibehenate (TDB) also failed to elicit any antibody production. TDB does not act on TLR-4, which underscores the importance of MPL in immune activation of the liposomal vaccine system. When MPER-His and Ni-NTA liposomes were used, a weak antibody titer of less than 10^3 was achieved, consistent with previous reports.[47] However, when Co-PoP liposomes were used, a greater titer by 2 orders of magnitude was observed. Presumably, the stable binding of the peptide to the liposomes in vivo was directly responsible for this effect. The Co-PoP immunization strategy was effective, with antibody titers persisting for at least 3 months, whereas no antibodies were detected with Ni-NTA liposomes after one month (Fig. 6c).

Post vaccination sera from mice was pooled and purified using Protein G agarose to yield purified IgG. This was then used to assess inhibition of viral entry by HIV (Fig. 6d). When the purified IgG from vaccinated mice was used at a final concentration of 0.2 mg/mL, viral entry was inhibited by more than 75 %. This efficacy of inhibition was greater than that of the broadly neutralizing monoclonal antibody 2F5 when incubated at a concentration of 2 μg/mL but less than when incubated at 20 μg/mL. These data show the potential for a vaccination approach making use of Co-PoP liposomes with HIV-derived peptides in order to induce antibody generation that can prevent viral entry.

Conclusion

Co-PoP and structures formed thereof represent a simple and versatile material for binding his-tagged proteins and peptides. This coating can easily confer targeting or immunogenic properties to diverse materials. This approach enables leverage of his-tagged polypeptides produced through modern peptide synthesis and genetic engineering. These can be easily, reliably and stably inserted into Co-PoP liposomes and other bilayer-coated materials for applications in biological systems.

Materials and Methods

See Supplementary Information for full methods.

Polypeptides

Custom peptides were obtained from commercial sources (see Supplementary Table 1). The recombinant heptahistidine-tagged cerulean-venus fusion protein was produced as previously described.[48]

PoP-liposomes

Freebase (2H) PoP was synthesized as previously described.[23] Metallo-PoPs were generated by incubating excess metal acetates with PoP in methanol or tetrahydrofuran. Reaction completion was monitored by thin layer chromatography. The solvent was then removed by rotary evaporation and PoP was extracted thrice with a chloroform:methanol:water mixture. Identity was confirmed with mass spectrometry. PoP-liposomes were created with the thin film method and extruded through 100 nm membranes using a handheld extruder. Stoichiometry approximations were based on the assumption that each ~100 nm liposome contains 80,000 lipids. For protein and peptide binding analysis, liposomes were formed with 10 molar % PoP along with 85 molar % DOPC (Avanti # 850375P), and 5 molar % PEG-lipid (Avanti # 880120P). Ni-NTA liposomes included 10 molar % Ni-NTA lipid dioleoyl-glycero-Ni-NTA (Avanti # 790404P) as well as 10 molar % 2H-PoP. Sulforhodamine B (VWR # 89139-502) liposomes contained 10 molar % PoP, 35 molar % cholesterol (Avanti # 700000P), 55 molar % DOPC and PEG-lipid as indicated. For bilayer integrity, cell binding and in vivo studies, 50 mM dye was used, whereas microscopy studies used 10 mM dye.

Polypeptide binding

1 μg of fluorescent reporter protein was incubated with 20 μg of liposomes in 200 μL phosphate buffered saline (PBS). Fluorescence in the FRET channel was measured and data were normalized to the FRET signal of the protein without addition of liposomes. EMSA experiments were performed using 2.5 μg protein incubated with 50 μg liposomes. For imidazole displacement experiments, 1 μg reporter protein was bound to 20 μg liposomes. Imidazole was then titrated and binding was assessed with fluorescence. For serum stability, 1 μg of reporter protein was bound to 20 μg liposomes in 100 μL PBS and then an equal volume of fetal bovine serum (FBS) was added and binding was monitored with fluorescence. Peptide binding was assessed with RGD-His FAM fluorophore quenching following incubation of 500 ng peptide with 20 μg liposomes.

Targeting experiments

2×10^4 U-87 and MCF-7 cells were seeded overnight in a 96-well plate. 500 ng RGD-His peptide was bound with 20 μg of sulforhodamine B-loaded liposomes which were incubated with cells for 2 h. Media was removed, cells were washed and liposomal uptake was assessed by fluorescence of sulforhodamine B following lysis with a 1 % Triton X-100 solution. For confocal imaging, 10^4 cells were seeded overnight in a chamber slide and 20 μg of liposomes were then added to the serum-containing media and incubated for 2 hours. Media was removed and cells were washed prior to confocal microscopy. Animal procedures were conducted in accordance with the policies of the University at Buffalo Institutional Animal Care and Use Committee. 5-week old female athymic nude mice

bearing U87 flank tumors (~5 mm) were intravenously injected with 200 μL of sulforhodamine B-loaded liposomes with or without cRGD-His. 45 minutes after injection, mice were sacrificed, organs were extracted, homogenized in a 0.2 % Triton X-100 solution and fluorescence was assessed to determine biodistribution.

Vaccinations

8-week-old female BALB/c mice (Harlan Laboratories) received hind ventral footpad injections on days 0 and 14 containing 25 μg of MPER peptide in 50 μL of sterile PBS. Where indicated, injections also included 25 μg MPL incorporated into the liposomes (Avanti # 699800P). Anti-MPER titer was assessed by ELISA in 96-well streptavidin-coated plates (GBiosciences #130804). 1 μg of his-tag-free MPER-biotin in 100 μL of PBS containing 0.1% Tween-20 (PBS-T) was incubated in the wells for 2 h at 37°C. Wells were washed and mouse sera was diluted in PBS containing 0.1% casein and incubated. Wells were then washed with PBS-T and goat anti-mouse IgG-HRP (GenScript # A00160) was added. The wells were washed again with PBS-T before addition of tetramethylbenzidine (Amresco # J644). Titers were defined as the reciprocal serum dilution at which the absorbance at 450 nm exceeded background by greater than 0.05 absorbance units. Every sample was averaged from duplicate measurements.

Viral entry experiments

Viral entry experiments were carried out as previously described.[49] Sera from 3 mice immunized with MPER and Co-PoP liposomes was pooled and IgG was isolated using immobilized Protein G beads (VWR # PI20398) according to vendor protocol. 2F5 was graciously provided by the free NIH AIDS reagent program. 1×10^4 TZM-bl receptor cells per well were plated in a 96-well plate the day before infection. HIV (multiplicity of infection of 0.1) was incubated with antibodies for 30 min at 37 °C, added to the cells and spinoculated at 1000×g for 1 h at 25 °C followed by further incubation for 2 days at 37 °C. Cell viability and viral entry were respectively assessed using the CellTiter-Fluor (Promega) and One-Glo (Promega) assays according to manufacturer protocol.

Supplementary Material

Refer to Web version on PubMed Central for supplementary material.

Acknowledgments

The authors thank Janet R. Morrow and Richard B. Bankert for valuable discussions, Alan Siegel for assistance with confocal microscopy, and the NIH AIDS Reagent Program. This work was supported by grants from the National Institutes of Health (R01EB017270, DP5OD017898 and HL77258).

References

1. Brannon-Peppas L, Blanchette JO. Nanoparticle and targeted systems for cancer therapy. Adv Drug Deliv Rev. 2012:206–212.
2. Purcell AW, McCluskey J, Rossjohn J. More than one reason to rethink the use of peptides in vaccine design. Nat Rev Drug Discov. 2007; 6:404–414. [PubMed: 17473845]
3. Canalle LA, Löwik DWPM, van Hest JCM. Polypeptide-polymer bioconjugates. Chem Soc Rev. 2010; 39:329–353. [PubMed: 20023856]

4. Nobs L, Buchegger F, Gurny R, Allémann E. Current methods for attaching targeting ligands to liposomes and nanoparticles. J Pharm Sci. 2004; 93:1980–1992. [PubMed: 15236448]
5. Algar WR, et al. The Controlled Display of Biomolecules on Nanoparticles: A Challenge Suited to Bioorthogonal Chemistry. Bioconjug Chem. 2011; 22:825–858. [PubMed: 21585205]
6. Sapra P, Allen TM. Ligand-targeted liposomal anticancer drugs. Prog Lipid Res. 2003; 42:439–462. [PubMed: 12814645]
7. Kirpotin D, et al. Sterically Stabilized Anti-HER2 Immunoliposomes: Design and Targeting to Human Breast Cancer Cells in Vitro. Biochemistry. 1997; 36:66–75. [PubMed: 8993319]
8. Yang T, et al. Preparation and evaluation of paclitaxel-loaded PEGylated immunoliposome. J Control Release. 2007; 120:169–177. [PubMed: 17586082]
9. Mastrobattista E, Koning GA, Storm G. Immunoliposomes for the targeted delivery of antitumor drugs. Adv Drug Deliv Rev. 1999; 40:103–127. [PubMed: 10837783]
10. Said Hassane F, Frisch B, Schuber F. Targeted Liposomes: Convenient Coupling of Ligands to Preformed Vesicles Using ‘Click Chemistry’. Bioconjug Chem. 2006; 17:849–854. [PubMed: 16704226]
11. Watson DS, Szoka FC Jr. Role of lipid structure in the humoral immune response in mice to covalent lipid–peptides from the membrane proximal region of HIV-1 gp41. Vaccine. 2009; 27:4672–4683. [PubMed: 19520200]
12. Liang MT, Davies NM, Toth I. Encapsulation of lipopeptides within liposomes: Effect of number of lipid chains, chain length and method of liposome preparation. Int J Pharm. 2005; 301:247–254. [PubMed: 16054787]
13. Pihlgren M, et al. TLR4- and TRIF-dependent stimulation of B lymphocytes by peptide liposomes enables T cell–independent isotype switch in mice. Blood. 2013; 121:85–94. [PubMed: 23144170]
14. Blanco-Canosa JB, et al. Recent progress in the bioconjugation of quantum dots. Coord Chem Rev. 2014; 263–264:101–137.
15. Terpe K. Overview of tag protein fusions: from molecular and biochemical fundamentals to commercial systems. Appl Microbiol Biotechnol. 2003; 60:523–533. [PubMed: 12536251]
16. Arnau J, Lauritzen C, Petersen GE, Pedersen J. Current strategies for the use of affinity tags and tag removal for the purification of recombinant proteins. Protein Expres Purif. 2006; 48:1–13.
17. Kubalek EW, Le Grice SFJ, Brown PO. Two-Dimensional Crystallization of Histidine-Tagged, HIV-1 Reverse Transcriptase Promoted by a Novel Nickel-Chelating Lipid. J Struct Biol. 1994; 113:117–123. [PubMed: 7536435]
18. Dorn IT, Neumaier KR, Tampé R. Molecular Recognition of Histidine-Tagged Molecules by Metal-Chelating Lipids Monitored by Fluorescence Energy Transfer and Correlation Spectroscopy§. J Am Chem Soc. 1998; 120:2753–2763.
19. Hussein WM, Ross BP, Landsberg MJ, Hankamer B, McGeary RP. Synthetic Approaches to Functionalized Lipids for Protein Monolayer Crystallizations. Curr Org Chem. 2009; 13:1378–1405.
20. Platt V, et al. Influence of Multivalent Nitrilotriacetic Acid Lipid–Ligand Affinity on the Circulation Half-Life in Mice of a Liposome-Attached His_6 -Protein. Bioconjug Chem. 2010; 21:892–902. [PubMed: 20384362]
21. Rüger R, Müller D, Fahr A, Kontermann RE. In vitro characterization of binding and stability of single-chain Fv Ni-NTA-liposomes. J Drug Target. 2006; 14:576–582. [PubMed: 17050123]
22. Xie J, Lee S, Chen X. Nanoparticle-based theranostic agents. Adv Drug Deliv Rev. 2010; 62:1064–1079. [PubMed: 20691229]
23. Lovell JF, et al. Porphysome nanovesicles generated by porphyrin bilayers for use as multimodal biophotonic contrast agents. Nat Mater. 2011; 10:324–332. [PubMed: 21423187]
24. Lovell JF, et al. Enzymatic Regioselection for the Synthesis and Biodegradation of Porphysome Nanovesicles. Angew Chem Int Ed. 2012; 51:2429–2433.
25. Carter KA, et al. Porphyrin–phospholipid liposomes permeabilized by near-infrared light. Nat Commun. 2014; 5
26. Rieffel J, et al. Hexamodal Imaging with Porphyrin-Phospholipid-Coated Upconversion Nanoparticles. Adv Mater. 2015; 27:1785–1790. [PubMed: 25640213]

27. Pasternack RF, Francesconi L, Raff D, Spiro E. Aggregation of nickel(II), copper(II), and zinc(II) derivatives of water-soluble porphyrins. Inorg Chem. 1973; 12:2606–2611.
28. Constable EC, Housecroft CE. Coordination chemistry: the scientific legacy of Alfred Werner. Chem Soc Rev. 2013; 42:1429–1439. [PubMed: 23223794]
29. Wegner SV, Spatz JP. Cobalt(III) as a Stable and Inert Mediator Ion between NTA and His6-Tagged Proteins. Angew Chem Int Ed. 2013; 52:7593–7596.
30. Terekhov SN, Galievsky VA, Chirvony VS, Turpin PY. Resonance Raman and absorption characterization of cationic Co(II)-porphyrin in its complexes with nucleic acids: binding modes, nucleic base specificity and role of water in Co(II) oxidation processes. J Raman Spectrosc. 2005; 36:962–973.
31. Ruoslahti E. Peptides as Targeting Elements and Tissue Penetration Devices for Nanoparticles. Adv Mater. 2012; 24:3747–3756. [PubMed: 22550056]
32. Pasqualini R, Koivunen E, Ruoslahti E. αv Integrins as receptors for tumor targeting by circulating ligands. Nat Biotechnol. 1997; 15:542–546. [PubMed: 9181576]
33. Danhier F, Breton AL, Préat V. RGD-Based Strategies To Target Alpha(v) Beta(3) Integrin in Cancer Therapy and Diagnosis. Mol Pharm. 2012; 9:2961–2973. [PubMed: 22967287]
34. Bloch S, et al. Targeting Beta-3 Integrin Using a Linear Hexapeptide Labeled with a Near-Infrared Fluorescent Molecular Probe. Mol Pharm. 2006; 3:539–549. [PubMed: 17009853]
35. Cai W, et al. Peptide-Labeled Near-Infrared Quantum Dots for Imaging Tumor Vasculature in Living Subjects. Nano Lett. 2006; 6:669–676. [PubMed: 16608262]
36. Hong G, et al. Near-Infrared-Fluorescence-Enhanced Molecular Imaging of Live Cells on Gold Substrates. Angew Chem Int Ed. 2011; 50:4644–4648.
37. Janib SM, Moses AS, MacKay JA. Imaging and drug delivery using theranostic nanoparticles. Adv Drug Deliv Rev. 2010; 62:1052–1063. [PubMed: 20709124]
38. Sperling RA, Gil PR, Zhang F, Zanella M, Parak WJ. Biological applications of gold nanoparticles. Chem Soc Rev. 2008; 37:1896–1908. [PubMed: 18762838]
39. Tam NCM, Scott BMT, Voicu D, Wilson BC, Zheng G. Facile Synthesis of Raman Active Phospholipid Gold Nanoparticles. Bioconjug Chem. 2010; 21:2178–2182. [PubMed: 21090645]
40. Zwick MB, et al. Broadly Neutralizing Antibodies Targeted to the Membrane-Proximal External Region of Human Immunodeficiency Virus Type 1 Glycoprotein gp41. J Virol. 2001; 75:10892–10905. [PubMed: 11602729]
41. Zwick MB. The membrane-proximal external region of HIV-1 gp41: a vaccine target worth exploring. AIDS. 2005; 19:1725–1737. [PubMed: 16227780]
42. Montero M, Houten NE, van Wang X, Scott JK. The Membrane-Proximal External Region of the Human Immunodeficiency Virus Type 1 Envelope: Dominant Site of Antibody Neutralization and Target for Vaccine Design. Microbiol Mol Biol Rev. 2008; 72:54–84. [PubMed: 18322034]
43. Burton DR, et al. HIV vaccine design and the neutralizing antibody problem. Nat Immunol. 2004; 5:233–236. [PubMed: 14985706]
44. Alam SM, et al. Role of HIV membrane in neutralization by two broadly neutralizing antibodies. Proc Natl Acad Sci. 2009; 106:20234–20239. [PubMed: 19906992]
45. Matyas GR, et al. Neutralizing antibodies induced by liposomal HIV-1 glycoprotein 41 peptide simultaneously bind to both the 2F5 or 4E10 epitope and lipid epitopes. AIDS. 2009; 23:2069–2077. [PubMed: 19710597]
46. Verkoczy L, et al. Induction of HIV-1 Broad Neutralizing Antibodies in 2F5 Knock-in Mice: Selection against Membrane Proximal External Region–Associated Autoreactivity Limits T-Dependent Responses. J Immunol. 2013; 191:2538–2550. [PubMed: 23918977]
47. Watson DS, Platt VM, Cao L, Venditto VJ, Szoka FC. Antibody Response to Polyhistidine-Tagged Peptide and Protein Antigens Attached to Liposomes via Lipid-Linked Nitrilotriacetic Acid in Mice. Clin Vaccine Immunol. 2011; 18:289–297. [PubMed: 21159923]
48. Dayananda KM, Gogia S, Neelamegham S. Escherichia coli-derived von Willebrand factor-A2 domain fluorescence/Förster resonance energy transfer proteins that quantify ADAMTS13 activity. Anal Biochem. 2011; 410:206–213. [PubMed: 21146487]

49. Yi HA, Diaz-Aguilar B, Bridon D, Quraishi O, Jacobs A. Permanent Inhibition of Viral Entry by Covalent Entrapment of HIV gp41 on the Virus Surface. Biochemistry. 2011; 50:6966–6972. [PubMed: 21736372]

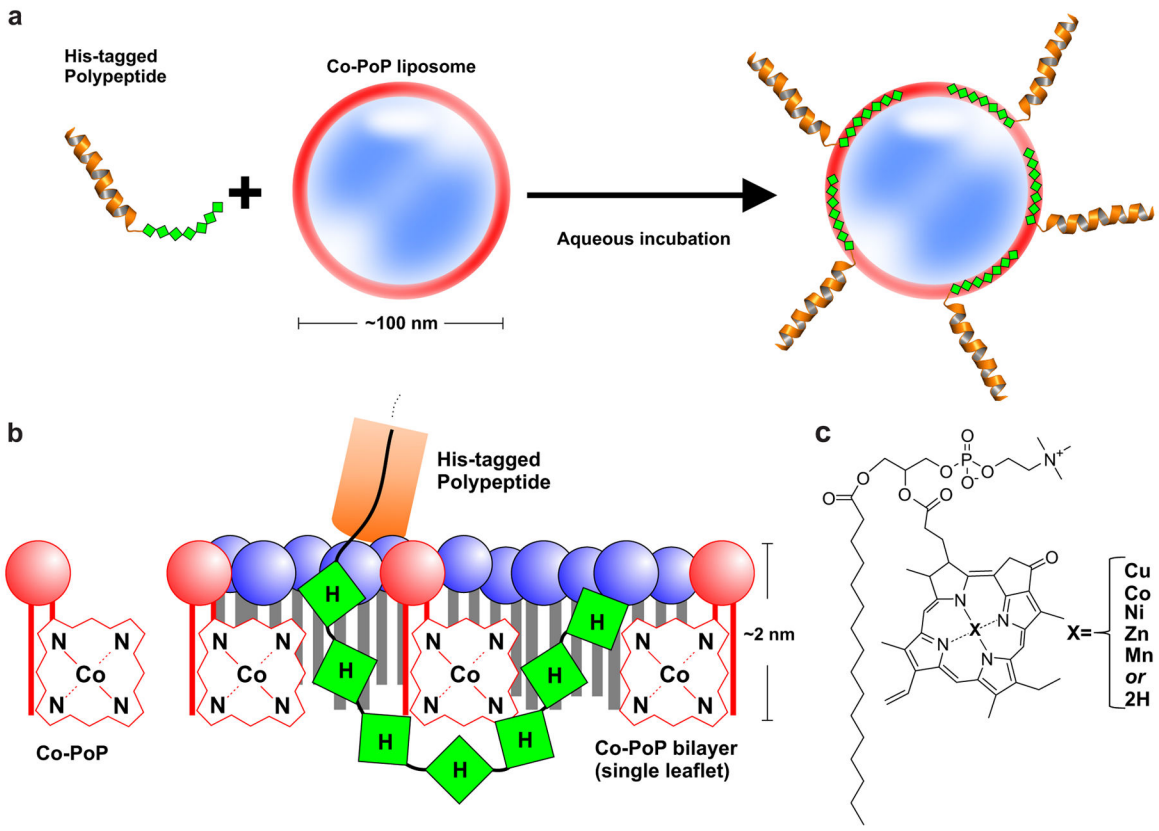

Figure 1. His-tagged polypeptides bind and functionalize Co-PoP-bilayers

a) Schematic showing a peptide with a his-tag (green) binding to preformed Co-PoP liposomes in aqueous solution. Simple aqueous incubation results in insertion of the his-tag into the bilayer, leading to stable binding. b) Insertion of a his-tagged polypeptide into a bilayer containing Co-PoP (red), along with a majority of conventional phospholipids (blue). Only a single leaflet of the bilayer is shown. The imidazole groups of the histidine residues coordinate with cobalt within the hydrophobic bilayer phase. c) Chemical structure of metallo-PoPs used in this study.

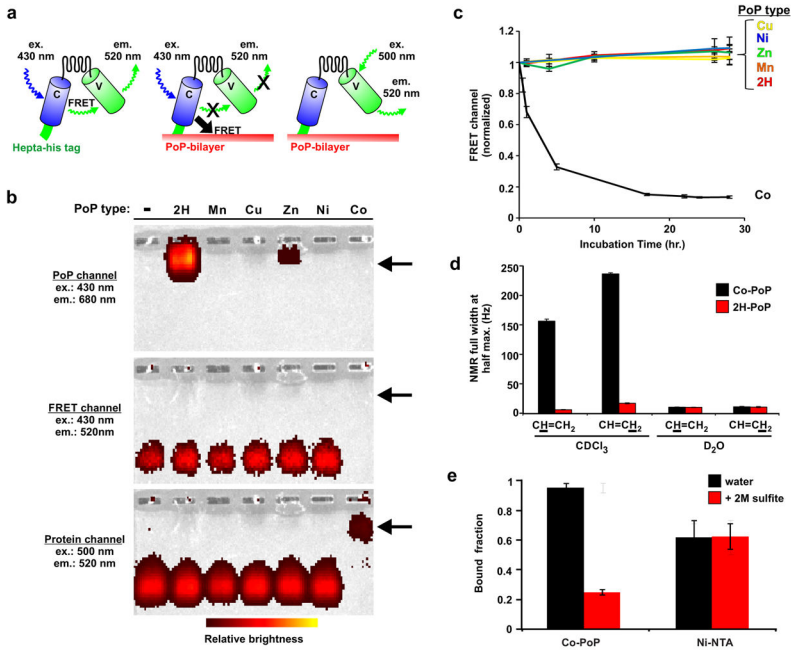

Figure 2. His-tagged protein binding to Co(III)-PoP liposomes

a) A heptahis-tagged fluorescence protein comprising Cerulean (C) fused to Venus (V) reveals binding to PoP-bilayers. When C is excited, FRET occurs and V emits fluorescence (left), but this is inhibited when bound to the PoP-bilayer due to competing FRET with the photonic bilayer (middle). C fluorescence can be directly probed even when the protein is bound to the bilayer (right). **b)** Multispectral fluorescence images of fusion protein electrophoretic mobility shift following incubation with indicated metallo-PoP liposomes. **c**) Binding kinetics of the fusion protein to the indicated metallo-PoP liposomes based on loss of C to V FRET. **d)** NMR peak widths of the underlined proton of the vinyl group on Co-PoP demonstrate paramagnetic broadening of Co (II) in deuterated chloroform ($CDCl_3$) but non-paramagnetic peaks of Co (III) following Co-PoP-liposome formation in deuterated water. **e)** Reversal of his-tagged peptide binding to Co-PoP liposomes following addition of 2 M sodium sulfate. Liposomes were formed with 10 molar % Co-PoP or Ni-NTA phospholipid. All graphs show means +/− std. dev. for n=3.

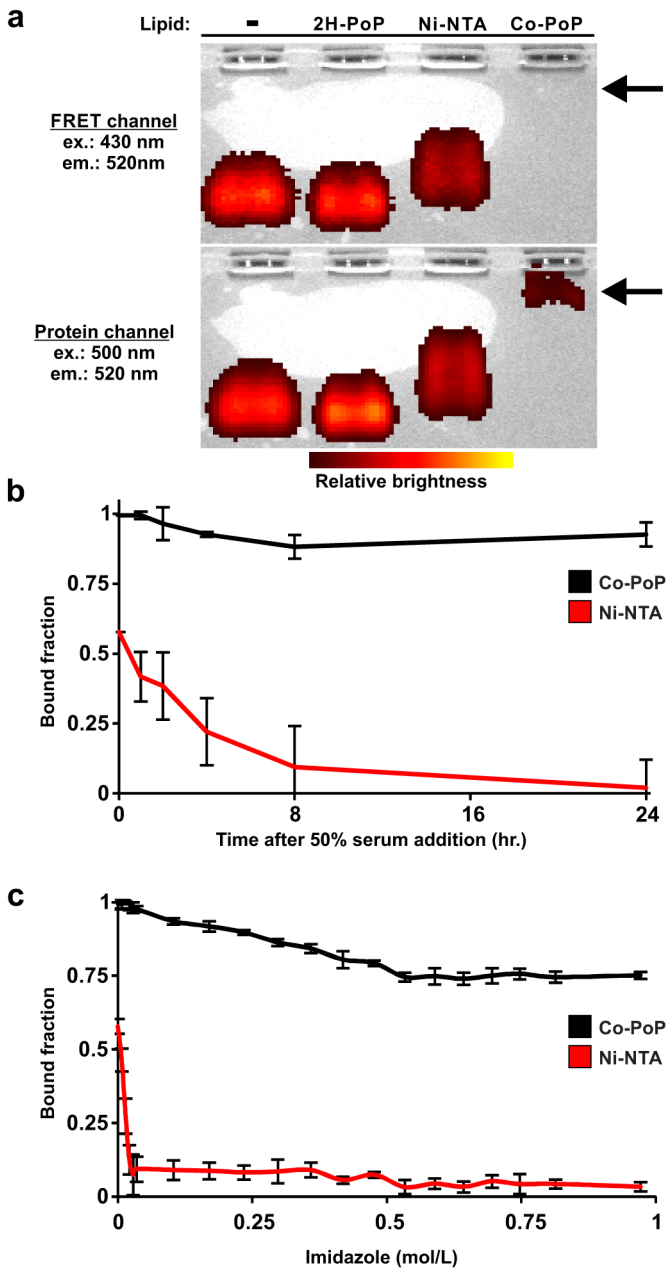

Figure 3. Robust his-tagged protein binding to Co-PoP liposomes

a) Multispectral electrophoretic mobility shift images of the fluorescent reporter protein incubated with liposomes containing the indicated lipid. The arrow points to the his-tagged protein bound to Co-PoP liposomes, which exhibits inhibited electrophoretic mobility due to the large size of the complex. 2H-PoP liposomes and Ni-NTA-liposomes did not stably bind the protein. b) Binding stability of the reporter protein bound to the indicated liposomes following addition of serum. **c)** Binding stability of the reporter protein bound to the indicated liposomes with excess free imidazole. All graphs show means +/− std. dev. for n=3.

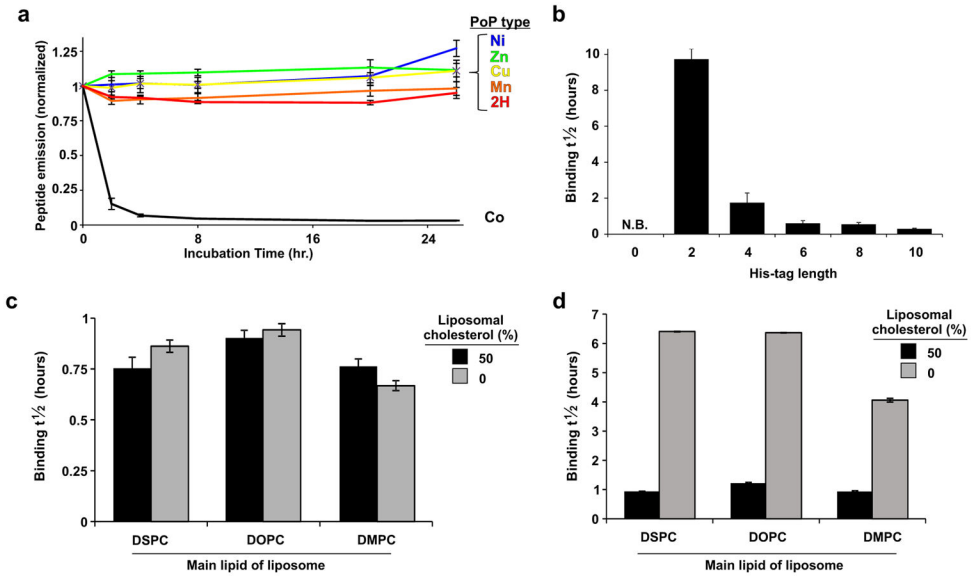

Figure 4. Binding of a short his-tagged RGD peptide to Co-PoP liposomes

a) Binding of a short linear RGD-His peptide labeled with FAM to metallo-PoP liposomes. Only Co-PoP liposomes bound the peptide. **b**) Effect of his-tag length on binding half-time to Co-PoP liposomes. No binding "N.B." was observed for the peptide lacking a his-tag. Increasing his-tag length resulted in faster binding. Effect of liposome composition on binding half-time to Co-PoP liposomes of indicated composition when incubated in PBS (**c**) or in 5 mg/mL BSA (**d**). In the presence of BSA, binding was slower for liposomes lacking cholesterol. All graphs show means +/− std. dev. for n=3.

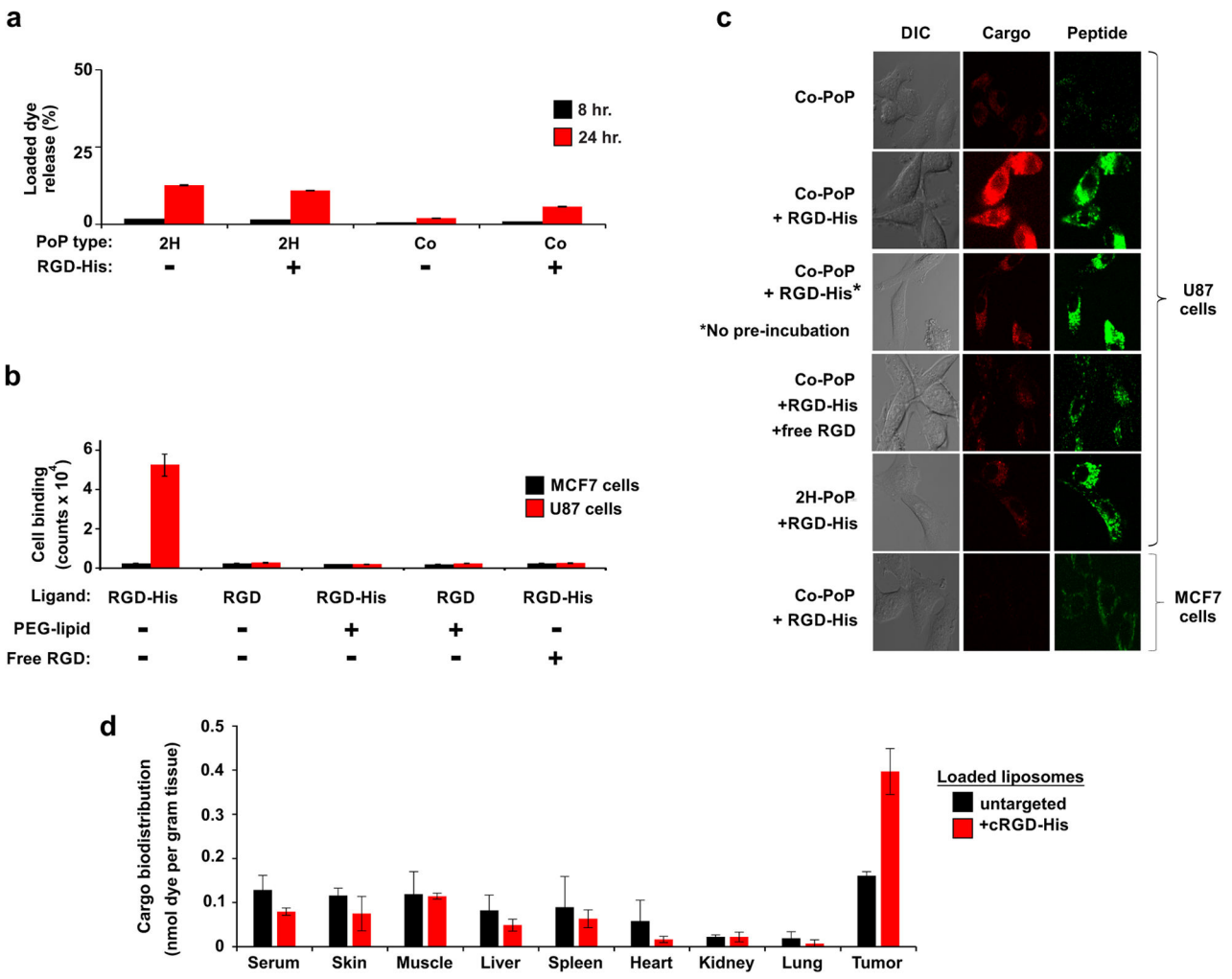

Figure 5. RGD-His targeting of cargo-loaded liposomes

a) Release of entrapped sulforhodamine B in preformed PoP liposomes. Minimal membrane destabilization occurred in the process of his-tagged peptide functionalization. **b)** Targeted uptake of sulforhodamine B-loaded liposomes in U87 cells known to express $\alpha_V\beta_3$ or MCF7 control cells. Cells were incubated in the indicated conditions and uptake was assessed by examining sulforhodamine B fluorescence. **c)** Confocal micrographs showing liposome uptake. Cells were incubated with the indicated liposome solutions for 2 hours, washed and imaged. All images were acquired with the same settings. **d)** Biodistribution of sulforhodamine B entrapped in Co-PoP liposomes with or without attachment of a his-tagged cyclic RGD targeting peptide 45 minutes following injection into nude mice bearing subcutaneous U87 tumors. All graphs show means +/− std. dev. for n=3

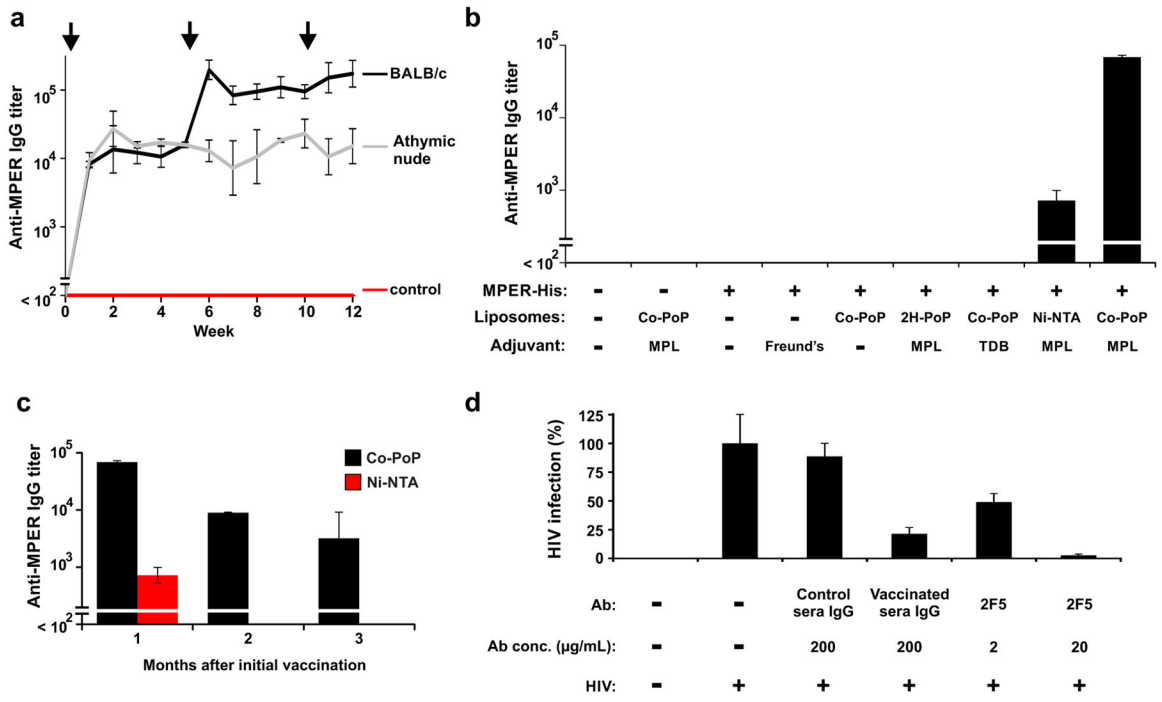

Figure 6. HIV peptide vaccination using immunogenic Co-PoP liposomes

a) BALB/c or athymic nude mice were immunized with Co-PoP liposomes containing a 25 μg of MPL and 25 μg of his-tagged MPER peptide derived from the HIV gp41 envelope protein. Sera titer was assessed with an ELISA using a biotinylated MPER peptide lacking a his-tag and probed with an anti-IgG secondary antibody. Arrows indicate time of vaccinations. Means +/− std. dev. for n=4 mice per group **b)** Anti-MPER titer in BALB/c mice vaccinated as indicated. Mice were vaccinated on week 0 and week 2 and serum was collected on week 4. Means +/− std. dev. for n=4 mice per group. **c)** Sustained anti-MPER titer in mice vaccinated with Co-PoP liposomes containing MPL relative to Ni-NTA liposomes containing MPL. Means +/− std. dev. for n=4 mice per group. **d)** Neutralization of HIV infection in 293T cells in the presence of indicated antibodies. Following vaccination using Co-PoP, IgGs were purified from pooled mouse sera using Protein A. The broadly neutralizing antibody 2F5 was used as a control. Means +/− std. dev. for n=3.